https://doi.org/10.5194/egusphere-2022-1067
Preprint. Discussion started: 14 October 2022
© Author(s) 2022. CC BY 4.0 License.

Seasonal to interannual variabilities of sea–air CO_2 exchange across Tropical Maritime Continent indicated by eddy–permitting coupled OGCM experiment

Faisal Amri[1], Takashi Nakamura[1], Atsushi Watanabe[2], Aditya. R. Kartadikaria[3], and Kazuo Nadaoka[1]

[1] Transdisciplinary Science and Engineering Department, Tokyo Institute of Technology, Tokyo, Japan
[2] Ocean Policy Research Institute, The Sasakawa Peace Foundation, Japan
[3] Faculty of Earth Sciences and Technology, Oceanography Research Group, Institut Teknologi Bandung, Bandung, Indonesia

Correspondence to: Faisal Amri (amri.f.aa@m.titech.ac.jp/faisal.amri.os12@gmail.com)

Abstract. The lack of long–term observational data has limited research on sea–air CO_2 exchange variabilities in the Tropical Maritime Continent (TMC). To address the issue, we utilized a three–dimensional high–resolution physical–biogeochemical ocean numerical model and applied it to simulate sea–air CO_2 exchange in the region over the last decade (2010–2019). Some key features like atmospheric CO_2 source signature and high sea surface pCO_2 environment inside the TMC were captured by the model. Within the TMC, model results indicated strong CO_2 degassing along the south of Java associated with the seasonal cycle of the upwelling system. Abundant supply of inorganic carbon during upwelling season and strong wind speed results in CO_2 degassing that could reach as high as 30 gC m^{-2} $year^{-1}$ around the area. In addition to the region acting as a full–year atmospheric CO_2 source, the TMC also exhibited interannual modulation in both sea–air CO_2 flux and sea surface pCO_2 which can be related to the El Niño–Southern Oscillation (ENSO) and Indian Ocean Dipole (IOD). Large–scale anomalous strong CO_2 degassing and high sea surface pCO_2 from 2015 to 2016 in response to the 2015/2016 El Niño evolution was observed and dominated by modulation within the TMC. It is further found that modulation of CO_2 degassing related to IOD were confined along the west of south of Java with a higher magnitude compared with anomalies related to ENSO which shows larger spatial scale but lower in the magnitude. Study conducted here may provide insight about possible variabilities of sea–air CO_2 exchange in the area that still poorly represented in many global–scale modelling and reconstruction efforts.

https://doi.org/10.5194/egusphere-2022-1067
Preprint. Discussion started: 14 October 2022
© Author(s) 2022. CC BY 4.0 License.

1 Introduction

The Tropical Maritime Continent (TMC) region acts as a water passage that allows Pacific Ocean water to be transported to the Indian Ocean as part of thermohaline circulation, which modulates the global climate system (Gordon, 1986; Wyrtki, 1961). Located between the Indian and Pacific Ocean, the TMC area is subject to modulation caused by variabilities occurring in these two ocean basins, including the El Niño–Southern Oscillation (ENSO) in the tropical Pacific Ocean, and Indian Ocean Dipole (IOD) in the Indian Ocean (Ashok et al., 2003; Saji and Yamagata, 2003; Sprintall et al., 2014). Recent studies have confirmed that these climate modes influence the TMC area through sea–air interaction perturbation, which affects the rainfall rate and oceanic properties such as sea surface temperature, sea surface height, and circulation pattern (Delman et al., 2016; Pujiana et al., 2019, 2020; Saji and Yamagata, 2003; Siswanto et al., 2020; Sprintall et al., 2014; Susanto et al., 2001; Syamsudin et al., 2004).

Despite the progress, studies on oceanic carbon cycle dynamics in the area remain very limited compared to the number of oceanic carbon–related studies that are growing globally (Bakker et al., 2016; Key et al., 2004; Takahashi et al., 2002, 2009). Although one of the latest observations–based studies by Kartadikaria et al. (2015) on the compilation of sea surface CO_2 partial pressure (sea surface pCO_2) across the Indonesian seas could provide a general view of the atmospheric CO_2 sink/source characteristics, it still could not represent the actual seasonal cycle and response of the sea–air CO_2 exchange to large–scale climate variabilities. Typical sea surface pCO_2 underway measurements conducted in a short period are not reliable in capturing the low–frequency variabilities that usually develop within an interannual time scale or longer (Sutton et al., 2017b). A study by Hamzah et al. (2020) in western Indonesian seas later confirmed this issue by highlighting the possible variation in the carbonate system over seasonal and interannual timescales in the undersampled area. The recent development of empirical model (Iida et al., 2015) or machine learning (Landschützer et al., 2016) in estimating sea surface pCO_2 and sea–air CO_2 exchange is unfortunately producing a relatively coarse resolution for resolving the complex island configuration within the TMC and showed inconsistent atmospheric CO_2 sink/source signature with observations–based study. These constraints make it challenging to apprehend TMC sea–air CO_2 exchange variabilities at various time scales.

Several modelling studies have indicated that the sea surface pCO_2 and sea–air CO_2 flux exhibit apparent modulation related to climate variability. A modelling study by Chai et al. (2009) in the South China Sea showed that sea surface pCO_2 followed the seasonal variations of net primary productivity, which was inversely correlated with the sea surface temperature (SST) anomaly in the Eastern Tropical Pacific region (NINO3). Global–scale modelling by Obata and Kitamura (2003) emphasized the Tropical Pacific Ocean sea–air CO_2 flux, where the variability in the region related to ENSO contributed approximately 70% to the global variability. Similar global–scale modelling was conducted by Valsala et al. (2014); despite indicating differences in the contribution of Tropical Pacific sea–air CO_2 flux variabilities to global variabilities, the study still agrees to the extent that Tropical Pacific Ocean variability has a significant influence on global carbon cycle modulation. They further suggested a stronger influence of El Niño–Modoki (Ashok et al., 2007) on upper–carbon cycle variability in the western part of the Tropical Pacific, adjacent to the TMC. In their modelling study, Xiu and Chai (2014)

https://doi.org/10.5194/egusphere-2022-1067
Preprint. Discussion started: 14 October 2022
© Author(s) 2022. CC BY 4.0 License.

also addressed the significance of the Pacific Decadal Oscillation and North Pacific Gyre Oscillation in modulating the sea–air CO_2 flux across the North Pacific region, highlighting the variabilities in much lower frequency domains. These studies partly confirm the hypothesis about the possible low–frequency modulation of the sea–air CO_2 exchange, considering the proximity of the TMC to the area studied previously. One of the remaining questions concerns the modulation pattern related to the Indo–Pacific climate variability in the area, which this study attempts to address. Information regarding sea–air CO_2 exchange variabilities in the TMC can enhance our understanding about overall atmospheric CO_2 sink/source variations across the tropics and its contribution to the global carbon cycle.

A high–resolution coupled Ocean General Circulation Model (OGCM) with low–trophic ecosystem module was employed to further resolve the issue of elucidating the sea–air CO_2 exchange variability across the TMC. The model was forced by realistic high–temporal resolution atmospheric forcings to approach the actual ocean–atmosphere dynamics that occurred during the simulation period. We further focused the analysis between 2010 and 2019 to examine the interannual changes in sea surface pCO_2 and sea–air CO_2 flux in the region. The analysis period included extreme events, such as the 2015/2016 El Niño and the 2019 positive IOD (pIOD). Previous studies have indicated that unprecedented anomalies occur around the TMC associated with these extreme climate events (e.g., Lu and Ren, 2020; Pujiana et al., 2019) and thus, have become an interesting period to examine the sensitivity of the sea–air CO_2 exchange variabilities in the area to such anomalous climate events.

2 Model and datasets

2.1 Model description

The low–trophic ecosystem model employed here was based on carbon (C) and nutrient (phosphate, nitrate, ammonium) tracing, low–trophic ecosystem model developed by Nakamura et al. (2018). The model was embedded in the Coupled Ocean–Atmosphere–Wave and Sediment Transport (COAWST) modelling environment (Warner et al., 2010) with the Regional Ocean Modelling System (ROMS; Shchepetkin and McWilliams, 2005) as the OGCM. Note that although model in Nakamura et al. (2018) mainly focuses on coral reef ecosystem, application on regional scale modelling was possible by deactivating the coral reef model and mainly relies on the low–trophic ecosystem compartment which further modified in this study. The low–trophic ecosystem model includes three phytoplankton functional types (PFT) in terms of carbon biomass, comprising diatoms, dinoflagellates, and coccolithophores. These PFTs utilize nutrients and total dissolved inorganic carbon (DIC) for photosynthesis and assimilation with dissolved oxygen as a by–product. The PFTs were distinguished by different assimilation efficiency, mortality rate, sinking velocity, and survivability under zooplankton grazing. Additionally, coccolithophores PFT use total alkalinity in addition to the DIC for the calcification process to produce $CaCO_3$ shells which explicitly calculated in this model. Details of relevant parametrization used for each PFT in this study can be seen in Table 1.

https://doi.org/10.5194/egusphere-2022-1067
Preprint. Discussion started: 14 October 2022
© Author(s) 2022. CC BY 4.0 License.

The material excreted by PFTs following the assimilation process immediately enters the labile dissolved organic matter (labile–DOM) pool. All dead phytoplankton biomass enters the particulate organic matter pool as detritus (detritus–POM) and immediately sinks into a deeper layer in the water column. As for the dead coccolithophore biomass, the previously produced $CaCO_3$ from the calcification process enters the particulate inorganic matter ($CaCO_3$–PIM) pool and sinks into a deeper layer, like the detritus–POM. Estimated produced $CaCO_3$–PIM from coccolithophore dead biomass was adapted from Krumhardt et al. (2017, 2019) which incorporates the effect of nutrient limitation, water temperature, and dissolved CO_2 gas on calcification efficiency.

One type of zooplankton in terms of carbon biomass was assigned in this model which grazed on phytoplankton, labile–DOM, and detritus–POM. As in the phytoplankton, the dead bodies of zooplankton also entered the detritus–POM pool, with a small part entering the $CaCO_3$–PIM pool. The $CaCO_3$–PIM fraction from zooplankton dead biomass was based on Ishizu et al. (2019, 2020).

The decomposition process takes place in the labile–DOM pool to resupply the dissolved inorganic carbon, nitrogen (as ammonium), and phosphorus (as phosphate) needed by phytoplankton. The decomposition of detritus–POM transforms detritus–POM into labile–DOM and dissolved inorganic material compounds (i.e., DIC, phosphate, and ammonium) simultaneously. Nitrate in this model was recovered through the nitrification of ammonium. We applied the first order dissolution reaction equation for the dissolution process of $CaCO_3$–PIM with a seawater $CaCO_3$ saturation state that varied within the water column (Jansen et al., 2002; Sarmiento and Gruber, 2006). Here, the $CaCO_3$–PIM saturation state was approximated as the calcite saturation state, given that the main $CaCO_3$ produced in this model came from coccolithophores. Dissolution of $CaCO_3$–PIM resupply the DIC and alkalinity as well. Schematic figure of material flow in our low–trophic ocean ecosystem model can be seen in Figure 1. Details on model formulation and additional parameters used in this model can be seen in the supplementary section 1 (S1).

https://doi.org/10.5194/egusphere-2022-1067
Preprint. Discussion started: 14 October 2022
© Author(s) 2022. CC BY 4.0 License.

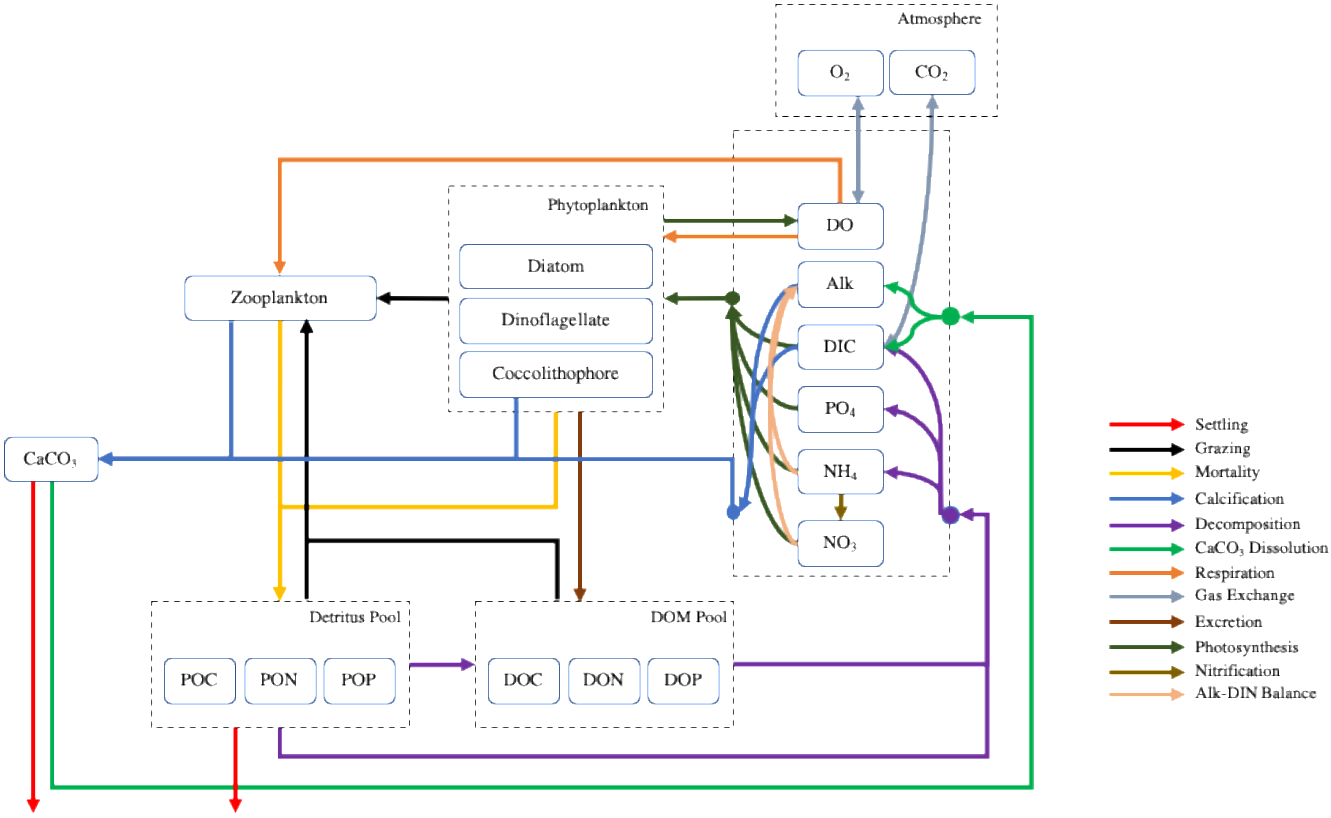

Figure 1. Schematic figure of low–trophic ecosystem model used in this study.

Sea surface pCO_2 was calculated in each time–step of simulation, set as 120 seconds, using modelled surface layer DIC, total alkalinity, water temperature, and salinity value following OCMIP protocol (Najjar and Orr, 1999). Exchange of CO_2 gas between sea surface and atmosphere further calculated by incorporating wind speed and difference between sea surface pCO_2 and atmosphere pCO_2 as in Wanninkhof (1992) with CO_2 solubility parameterization following Weiss (1974). By allowing the gas exchange, the DIC within the sea surface layer is subject to dynamics from sea–air interaction in addition to the biogeochemical processes within the seawater. The sea surface pCO_2 can be decomposed into four driving components of sea surface temperature (SST), sea surface salinity (SSS), sea surface total DIC (SSDIC), and sea surface total alkalinity (SSAlk) following Takahashi et al. (1993)

$$\mathrm{dpCO_2} = \left(\frac{\partial \mathrm{pCO_2}}{\partial \mathrm{SST}}\right)\mathrm{dSST} + \left(\frac{\partial \mathrm{pCO_2}}{\partial \mathrm{SSS}}\right)\mathrm{dSSS} + \left(\frac{\partial \mathrm{pCO_2}}{\partial \mathrm{SSDIC}}\right)\mathrm{dSSDIC} + \left(\frac{\partial \mathrm{pCO_2}}{\partial \mathrm{SSAlk}}\right)\mathrm{dSSAlk}$$

We set the model domain to span from the Southeast Tropical Indian Ocean (SETIO) to the Northwest Pacific Ocean (90°E–164°E; 18°S–29°N). The domain was gridded uniformly with a horizontal resolution of 1/6° × 1/6° while the water column was transformed into 30–layers of non–uniform, terrain–following s–coordinates. Simulation experiment was started from

https://doi.org/10.5194/egusphere-2022-1067
Preprint. Discussion started: 14 October 2022
© Author(s) 2022. CC BY 4.0 License.

December 2007 to January 2020. Results analysed in this study covers the 2010–2019 period considering the first two years simulation as spin–up period. Generic length scale (GLS) mixing parameterizations of the k–ε configuration were utilized in this model for vertical mixing combined with the Kantha–Clayson stability function (CPP options KANTHA_CLAYSON) and horizontal smoothing of buoyancy/shear (CPP options N2S2_HORAVG). Smagorinsky–like diffusion (CPP option UV_SMAGORINSKY and TS_SMAGORINSKY) was activated in this simulation for the horizontal diffusion and viscosity for both momentum and tracer variables.

Table 1. Relevant parameterizations for each phytoplankton functional types (PFT) used in simulation experiment. All values shown here were coarsely calibrated from Gregg et al. (2007) and Krumhardt et al. (2019).

	Dinoflagellate	Diatom	Coccolithophore
Maximum photosynthetic rate at 0°C (day^{-1})	0.44	0.50	0.47
Optimum light intensity ($J\ m^2\ s^{-1}$)	87	93	71
Maximum grazing rate by zooplankton at 0°C (day^{-1})	0.36	0.34	0.29
Threshold value for grazing by zooplankton ($\mu molC\ L^{-1}$)	0.054	0.072	0.082
PO_4 half saturation constant ($\mu mol\ L^{-1}$)	0.005	0.050	0.006
NO_3 half saturation constant ($\mu mol\ L^{-1}$)	0.20	0.50	0.20
NH_4 half saturation constant ($\mu mol\ L^{-1}$)	0.01	0.05	0.01
Sinking Velocity ($m\ day^{-1}$)	0.25	0.75	1.00

2.2 Model forcing

To generate the physical–biogeochemical ocean dynamics within the model domain, the model was by forced three main components consisted of tidal forcing, atmospheric forcing, and atmospheric CO_2 concentration. The Oregon State University TPXO tides model output (Egbert and Erofeeva, 2002) and 55–years Japan Reanalysis product (JRA–55; Kobayashi et al., 2015) as tidal forcing and atmospheric forcing, respectively, were used to generate the circulation dynamics (Physical aspect) in the model domain. Utilized atmospheric forcing here include the three–hourly surface air pressure, air temperature, humidity, wind speed, precipitation, and cloud fraction. Bulk fluxes (i.e., Shortwave radiation, longwave radiation, latent heat, and sensible heat) were computed internally in the model. Annual global–averaged atmospheric CO_2 concentration recorded in the NOAA Earth System Research Laboratory (NOAA ESRL) was used and applied uniformly across the entire model domain to generate the CO_2 exchange between sea surface and atmosphere (Biogeochemical aspect).

https://doi.org/10.5194/egusphere-2022-1067
Preprint. Discussion started: 14 October 2022
© Author(s) 2022. CC BY 4.0 License.

River discharge across the model domain was not implemented in this study; thus, the indicated results of pCO_2 and sea–air CO_2 flux were caused solely by the ocean–atmosphere interaction dynamics.

2.3 Model initialization and boundary condition

The circulation model was initialized using Global Ocean Forecasting System (GOFS) analysis/reanalysis product (Chassignet et al., 2006) which provides horizontal momentum ($u, v, \bar{u}, \bar{v}$), water temperature (T), water salinity (S), and sea surface height (η) information. Information in domain's boundary also provided by the same GOFS dataset. Initial and boundary condition for biogeochemical tracers were provided by analytically estimating the vertical profile of phytoplankton, zooplankton, DIC, Alkalinity, nutrients (Nitrate, Ammonium, and Phosphate), and dissolved oxygen. Analytical expression for necessary parameters in the low–trophic ecosystem model was established using Global Data Analysis Project 2nd version (GLODAPv2; Key et al., 2004) which stores scientific cruise data across the globe including some areas within modelling domain. Each of observed total DIC (Total CO_2 in GLODAPv2), total alkalinity, and dissolved oxygen were paired with observed water temperature to create a fourth–order polynomial equation using least–square method. The polynomial equation was later applied to the model's initial and boundary condition by using GOFS water temperature data.

The nutrients in the model's initial and boundary condition further calculated using linear relationship between salinity–normalized DIC and nutrient concentration indicated by the GLODAPv2 data adapting Sarmiento and Gruber (2006). The linear equation then utilized estimated DIC value and Salinity from the GOFS. We found that the C:P and C:N ratio of 131.9 and 9.2 which higher than Redfield ratio (Redfield, 1934) but still lower than contemporary estimation in Martiny et al. (2014). Observed C:P and C:N values from the GLODAPv2 were later used in the model as well. Through this approach, we could create initial condition in the area with sparse observation record such as the TMC. The initial and boundary condition for phytoplankton and zooplankton on the other hand, used simpler analytical approach where biomass was calculated as function of vertical position. More details on the analytical equations used to create the initial and boundary conditions of the low–trophic ecosystem model is provided in Table 2.

$$\mathrm{Phy(z)} = \frac{10.5 - 0.00095 \times (\mathrm{z} + 50)^2}{24} \quad \text{For } \mathrm{z} > -155 \text{ m}$$

$$\mathrm{Zoo(z)} = 0.1 \times \mathrm{Phy(z)}$$

Lateral boundary condition was set to be mixed radiation–nudging for the 3D momentum and tracer variables. The inflow nudging timescale for the temperature/salinity and biogeochemical tracers were set to 100 days and 180 days, respectively.

Table 2. Analytical equations used to estimate necessary biogeochemical parameters in initial and boundary conditions of the ecosystem model. For application in the simulation experiment, water temperature (T) and salinity (S) in the equations were obtained from the Global Ocean Forecasting System (GOFS) product.

https://doi.org/10.5194/egusphere-2022-1067
Preprint. Discussion started: 14 October 2022
© Author(s) 2022. CC BY 4.0 License.

Parameter (unit)	Equation
Dissolved inorganic carbon (μmol kg^{-1})	$2312.12 + (10.68 \times T) - (3.50 \times T^2) + (0.16 \times T^3) - (2.42 \times 10^{-3} \times T^4)$
Total alkalinity (μmol kg^{-1})	$2444.73 - (22.29 \times T) + (0.09 \times T^2) + (1.28 \times 10^{-3} \times T^3) + (4.60 \times 10^{-4} \times T^4)$
Dissolved oxygen (μmol L^{-1})	$245.85 - (52.01 \times T) + (6.46 \times T^2) - (0.28 \times T^3) + (3.84 \times 10^{-3} \times T^4)$
Nitrate (μmolN L^{-1})	$0.98 \times \frac{\left(\frac{(DIC \times 35)}{S} - 1977.4\right)}{9.77}$
Ammonium (μmolN L^{-1})	$0.02 \times \frac{\left(\frac{(DIC \times 35)}{S} - 1977.4\right)}{9.77}$
Phosphate (μmolP L^{-1})	$\frac{\left(\frac{(DIC \times 35)}{S} - 1961.3\right)}{141.23}$

3 Results

3.1 Overall sea–air CO_2 exchange features and comparison with other datasets

Comparison with Surface Ocean CO_2 Atlas (SOCAT; Bakker et al., 2016) over the 2010–2019 period shows that the model could capture the high sea surface pCO_2 environment within the TMC as shown from underway observation track in the Indonesia Throughflow area (Figure 2). Modeled sea surface pCO_2 inside the TMC also fell within the observed value by Kartadikaria et al. (2015) and Hamzah et al. (2020). They reported sea surface pCO_2 value inside the TMC that higher than 400 μatm and suggested the role of the region as a net atmospheric CO_2 source. However, the model still overestimates the sea surface pCO_2 in open ocean surrounding the TMC such as the Western Pacific Ocean. The striking sea surface pCO_2 gradient between open ocean and inner TMC was still reproduced by the model despite being much weaker than SOCAT data. Other dataset derived from empirical model (Iida et al. 2021) and machine learning (Landschützer et al., 2016; not shown) with 1° × 1° horizontal resolution did not exhibit such contrasting differences. Excess alkalinity in the sea surface, calculated as difference between total alkalinity and DIC, from simulation indicates that there is a considerable gradient between the TMC and surrounding open ocean which corresponds to higher sea surface pCO_2 inside the TMC compared with open ocean. Modeled excess alkalinity in the open ocean were still lower compared with reconstruction in Iida et al (2021) which may explain the higher–than–observed sea surface pCO_2 in the open ocean.

https://doi.org/10.5194/egusphere-2022-1067
Preprint. Discussion started: 14 October 2022
© Author(s) 2022. CC BY 4.0 License.

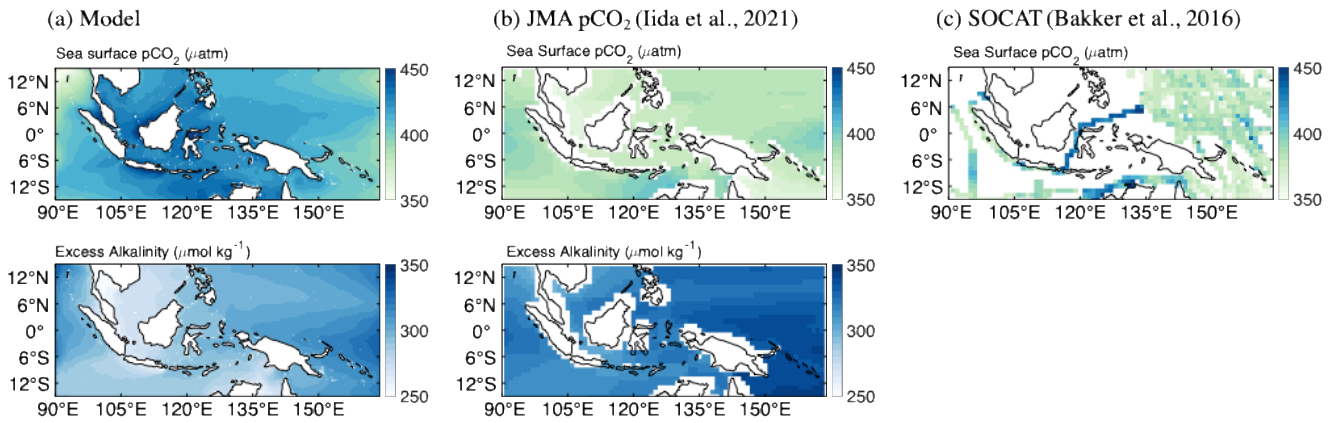

Figure 2. First row: Overall sea surface pCO_2 (in µatm) indicated by (a) Numerical model utilized in this study, (b) Global reconstruction product using empirical model (Iida et al., 2021), and observation archived in Surface Ocean CO_2 Atlas (SOCAT; Bakker et al., 2016). Second row: Sea surface excess alkalinity (in µmol kg^{-1}) as calculated by (a) Numerical model and (b) empirical model (Iida et al., 2021).

The atmospheric CO_2 sink/source characteristic over the 2010–2019 shows large spread between datasets as shown in Figure 3. Our model indicates that inside TMC acts as a net atmospheric CO_2 source with average flux of +0.42 mol m^{-2} $year^{-1}$ consistent with study by Kartadikaria et al. (2015) and Hamzah et al. (2020) which estimated the average CO_2 degassing rate of +0.33 mol m^{-2} $year^{-1}$ and +0.10 mol m^{-2} $year^{-1}$, respectively. Overall CO_2 source characteristic within the TMC produced by model here also in line with recent state–of–art global scale earth system model which incorporated coastal dynamics (Mathis et al., 2022). Other sea surface pCO_2 and sea–air CO_2 exchange reconstruction products in contrast, indicated the area as a net atmospheric CO_2 sink with average flux of –0.04 mol m^{-2} $year^{-1}$ (Iida et al., 2016) and –0.01 mol m^{-2} $year^{-1}$ (Landschützer et al., 2016), respectively. Note that in comparison with study conducted by Kartadikaria et al. (2015), study by Hamzah et al. (2020) utilized much shorter observation data and smaller area.

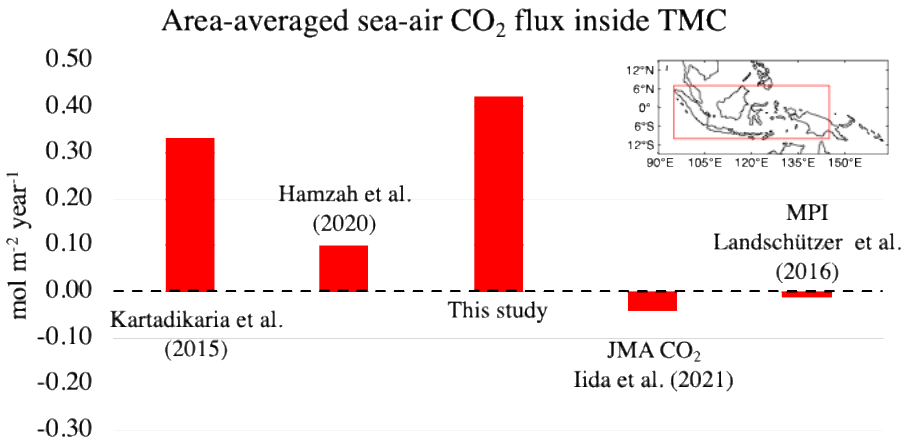

Figure 3. Estimated sea–air CO_2 flux (in mol m^{-2} $year^{-1}$) inside the TMC according to various studies and global reconstruction product. Positive and negative value indicates atmospheric CO_2 source and sink signature, respectively. Area used for calculating

https://doi.org/10.5194/egusphere-2022-1067
Preprint. Discussion started: 14 October 2022
© Author(s) 2022. CC BY 4.0 License.

the sea–air CO_2 flux from simulation experiment and global reconstruction products (i.e, Iida et al., 2021; Landschützer et al., 2016) is bounded by red line shown in upper–right map.

3.2 Seasonal pattern of sea–air CO_2 exchange

Figure 4 showed mean seasonal cycle of sea surface pCO_2 and sea–air CO_2 flux across the TMC between 2010–2019. During winter (December–February), model results show high sea surface pCO_2 around the Timor Sea along with strong CO_2 degassing to the atmosphere. In following spring (March–May), high sea surface pCO_2 is more distributed within the TMC from northern part to southern part of the region, including South China Sea and most of area in Indonesia sea. Strong CO_2 degassing however, did not apparent during the season as result from weak wind speed. Simulation results indicated strong CO_2 degassing appear again during Summer (June–August) particularly around South China Sea and South of Java along with high pCO_2 which can exceed 30 gC m^{-2} $year^{-1}$ and 466 µatm, respectively. High sea surface pCO_2 and strong CO_2 degassing around South of Java was further maintained until Autumn (September–November) making it the longest strong CO_2 degassing across the TMC region. The strong CO_2 degassing period in South of Java was coincided with upwelling season which previously observed by many studies (Horii et al., 2018; Ningsih et al., 2013: Siswanto et al., 2020; Susanto et al., 2001).

https://doi.org/10.5194/egusphere-2022-1067
Preprint. Discussion started: 14 October 2022
© Author(s) 2022. CC BY 4.0 License.

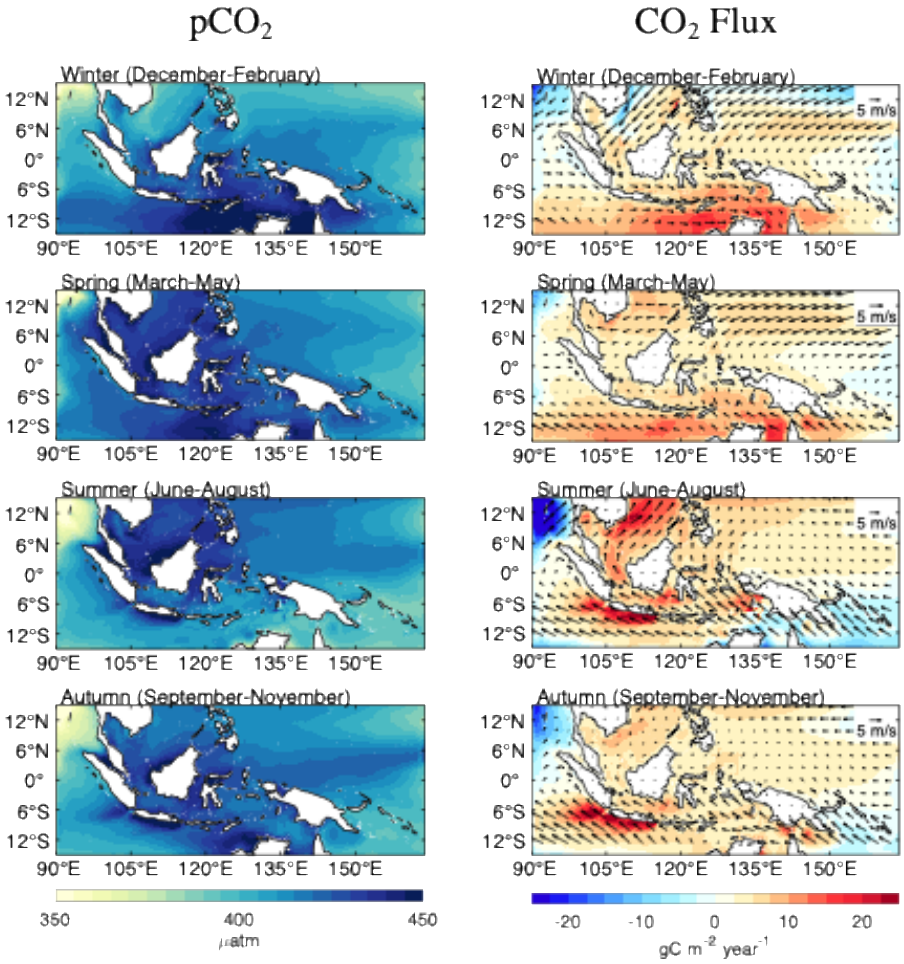

Figure 4. Mean seasonal cycle of sea surface pCO_2 (Left column figures; in μatm) and sea–air CO_2 flux (Right column figures, in gC m^{-2} $year^{-1}$). Positive and negative value in sea–air CO2 flux map indicates atmospheric CO_2 source and sink area, respectively.

Figure 5 shows the results of sea surface pCO_2 decomposition analysis following Takahashi et al. (1993). It was indicated that spatial variation of sea surface pCO_2 closely follows SST seasonality in the TMC. As the region located in the tropics, there is a clear interhemispheric difference of SST seasonal cycle in the northern and southern part of the region which led to alternating north–south gradient of sea surface pCO_2. The biological processes, represented by SSDIC and SSAlk, generally has weaker influence than the SST influence on large–scale sea surface pCO_2 seasonality as the effect of SSDIC and SSAlk on sea surface pCO_2 tends to cancel each other. With the exception on South of Java, the biological process in the region induced net increase(decrease) to the sea surface pCO_2 during the onset(termination) of upwelling. In those periods, the biological effect on sea surface pCO_2 was counteracted by the SST effect. We also noted that in comparison with the open ocean, our simulation results indicated the inner part of TMC region as biogeochemical activities 'hotspot' where influence

https://doi.org/10.5194/egusphere-2022-1067
Preprint. Discussion started: 14 October 2022
© Author(s) 2022. CC BY 4.0 License.

of SSDIC and SSAlk to sea surface pCO_2 was more notable. As expected for the sea surface salinity, changes in SSS showed smallest influence on the sea surface pCO_2 seasonality across the region compared with other three driving components.

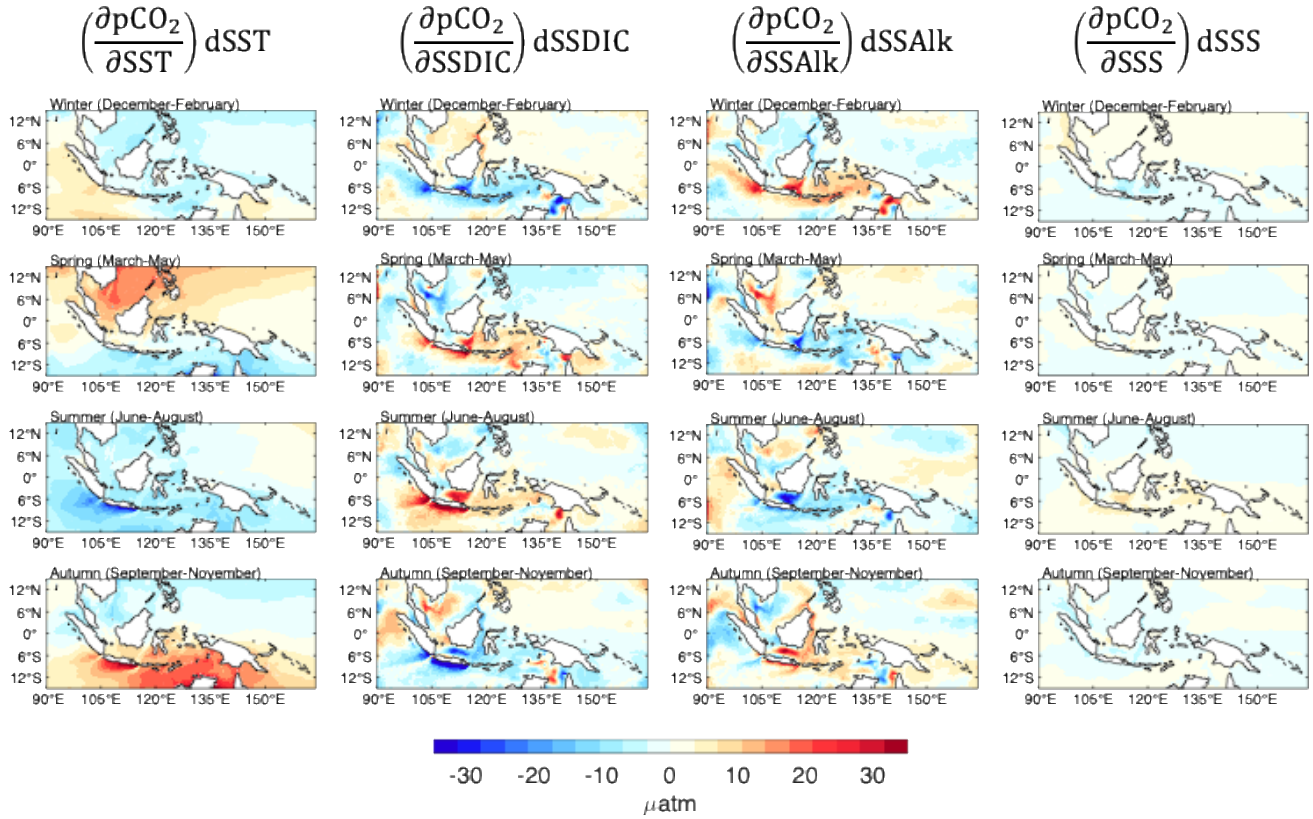

Figure 5. Decomposition of sea surface pCO_2 seasonality across the Tropical Maritime Continent (in µatm). From left column to right column figures: Changes in sea surface pCO_2 caused by sea surface temperature, sea surface DIC, sea surface Alkalinity, and sea surface salinity.

Upwelling in the South of Java reaches its annual peak in September as shown in the sea surface chlorophyll–a concentration from MODIS satellite (Hu et al., 2012) and phytoplankton carbon biomass from simulation results (Figure 6). Calculation of Chl:C ratio in the area shows an average value of 0.02 which within the range in study by Arteaga et al. (2016). The sea surface pCO_2 in the South of Java closely follow this upwelling seasonality with sea surface DIC become the main driving component for high sea surface pCO_2 during upwelling peak. On the other hand, strong CO_2 degassing to the atmosphere (~ 30 gC m^{-2} $year^{-1}$) lead the upwelling peak by one month (August) and maintained until succeeding month of September. Wind speed around the area according to JRA–55 showed its maxima in August which can explain the early strong CO_2 degassing prior to the upwelling peak. Although wind speed around south of Java showed relaxation starting from September, surface water with high inorganic carbon concentration further maintains the strong CO_2 degassing condition due to high sea surface pCO_2.

https://doi.org/10.5194/egusphere-2022-1067
Preprint. Discussion started: 14 October 2022
© Author(s) 2022. CC BY 4.0 License.

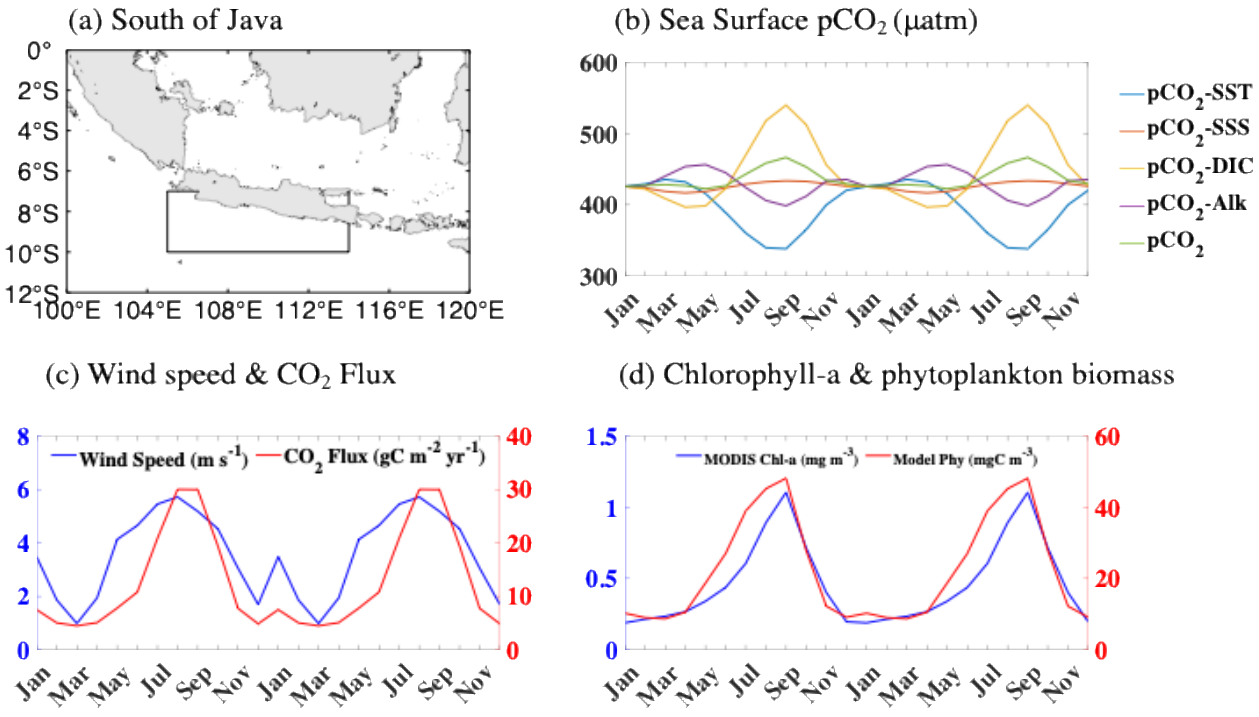

Figure 6. (a) South of Java map; (b) Modelled seasonal sea surface pCO_2 associated with its component (in µatm); (c) Seasonal wind speed around South of Java according to JRA–55 datasets (in m/s) and modelled sea–air CO_2 flux (in gC m^{-2} $year^{-1}$); (d) Modelled seasonal phytoplankton carbon biomass (mgC m^{-3}) and chlorophyll–a concentration (mg m^{-3}) according to Moderate Resolution Imaging Spectrometer (MODIS) satellite observation

3.3 Interannual variability over the last decade (2010–2019)

The interannual variability was examined by removing the mean seasonal cycle of simulated sea surface pCO_2 and sea–air CO_2 flux over the 2010–2019 period which later identified as anomalies. In addition to the secular trend caused by atmospheric CO_2 concentration growth used in the model forcing, modeled sea–air CO_2 flux showed notable interannual variation particularly between 2015–2016 and 2019 coincided with the development of 2015/2016 El Niño and 2019 pIOD (Figure 7). Those two major modulations in the sea–air CO_2 flux had shown to slow down the decreasing trend in the CO_2 flux over the study period (Figure 7a). The sea surface pCO_2 anomalies on the other hand, showed relative steady increase although some modulations like in the early 2016 can be observed. This again confirms that sea–air CO_2 exchange across the TMC also subject to low–frequency modulation which can be related to the Indo–Pacific climatic forcing.

https://doi.org/10.5194/egusphere-2022-1067
Preprint. Discussion started: 14 October 2022
© Author(s) 2022. CC BY 4.0 License.

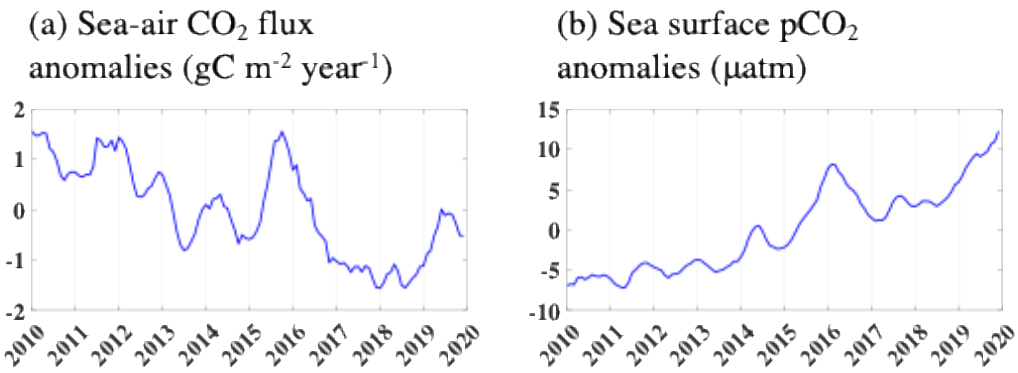

Figure 7. Five–months moving average of (a) sea–air CO_2 flux anomalies (in gC m^{-2} $year^{-1}$) and (b) sea surface pCO_2 anomalies (in μatm) across the 95ºE–164ºE; 15ºS–15ºN over the 2010–2019 period. Positive and negative values indicate higher–than–usual sea surface sea–air CO_2 flux/ pCO_2 and lower–than–usual relative to the mean seasonal cycle, respectively.

Quantification of Indo–Pacific climatic forcing influence on the sea–air CO_2 exchange across the TMC was conducted by regression analysis on sea surface pCO_2 anomalies, sea–air CO_2 flux anomalies, and wind speed anomalies. Considering that ENSO and IOD showed a statistically significant correlation over the 2010–2019 (Pujiana et al., 2019), we further separated the effect of ENSO on IOD and *vice versa* by performing partial correlation analysis for sea surface pCO_2 anomalies, sea–air CO_2 flux anomalies, and wind anomalies following the methods in Saji and Yamagata (2003) prior to the regression analysis. This will allow us to evaluate the extent of each climatic forcing effects on sea–air CO_2 exchange across the study region. The ENSO and IOD events were represented by central–eastern Pacific sea surface temperature anomaly 'NINO3.4' and dipole mode index 'DMI' (See Saji et al., 1999 for further details about DMI calculation), respectively from HadISST 1.1 (Rayner et al. 2003). For uniformity reasoning, we regressed the sea surface pCO_2 anomalies, sea–air CO_2 flux anomalies, and wind speed anomalies from JRA55 against one–standard deviation (± 1σ) of NINO3.4 ($\sigma_{NINO3.4}$ = 0.80 ºC) and DMI (σ_{DMI} = 0.26 ºC) over the 2010–2019 period. Note that typical ENSO mature phase occurs within the November–March period, while the IOD occurs in July–November. Thus, results presented in this section will be focused on these two–period which corresponds to each climatic event.

Regressed sea surface pCO_2 anomalies and sea–air CO_2 flux anomalies against one–standard deviation (± 1σ) of NINO3.4 and DMI revealed distinguishable spatial extents of modulation (Figures 8 and 9). Anomalies associated with ENSO during the November–March period tended to have a larger spatial extent, extended from SETIO region up to South China Sea, compared with IOD during July–November, which was confined along south of Java. Results from the regression analysis also showed an extended minor influence of IOD on the sea surface pCO_2 variabilities up to the lesser Sunda Island water area and inside the Indonesian seas.

Regressed sea surface pCO_2 anomalies against NINO3.4 further suggested a stronger sensitivity of the TMC to ENSO forcing compared with the adjacent Western Pacific Ocean denoted by the area which satisfy statistical significance threshold defined in this study (i.e., $p < 0.01$). The smaller extent of regressed sea–air CO_2 flux anomalies against NINO3.4 implies the nonlinearity between sea surface pCO_2 modulation and sea–air CO_2 exchange modulation in response to the same

https://doi.org/10.5194/egusphere-2022-1067
Preprint. Discussion started: 14 October 2022
© Author(s) 2022. CC BY 4.0 License.

climatic forcing which is possible considering the additional factor of wind speed that determine the sea–air CO_2 flux. Regression analysis conducted here suggested an anomalous sea surface pCO_2 and CO_2 degassing increase associated with associated with ENSO over the 2010–2019 can be as high as +40 µatm $(1\sigma NINO3.4)^{-1}$ and +5 gC m^{-2} $year^{-1}(1\sigma NINO3.4)^{-1}$. Exclusion of the 2015/2016 El Niño event in the regression analysis (Figure 8, second column) decreased the magnitude of the sea surface pCO_2 anomalies and significantly reduced the spatial extent of the sea–air CO_2 flux anomalies despite the occurrence of strong 2010–2012 La Niña. This further suggests that the double–dip La Niña in 2010/2011 and 2011/2012 induced less–pronounced sea–air CO_2 flux modulation within the TMC.

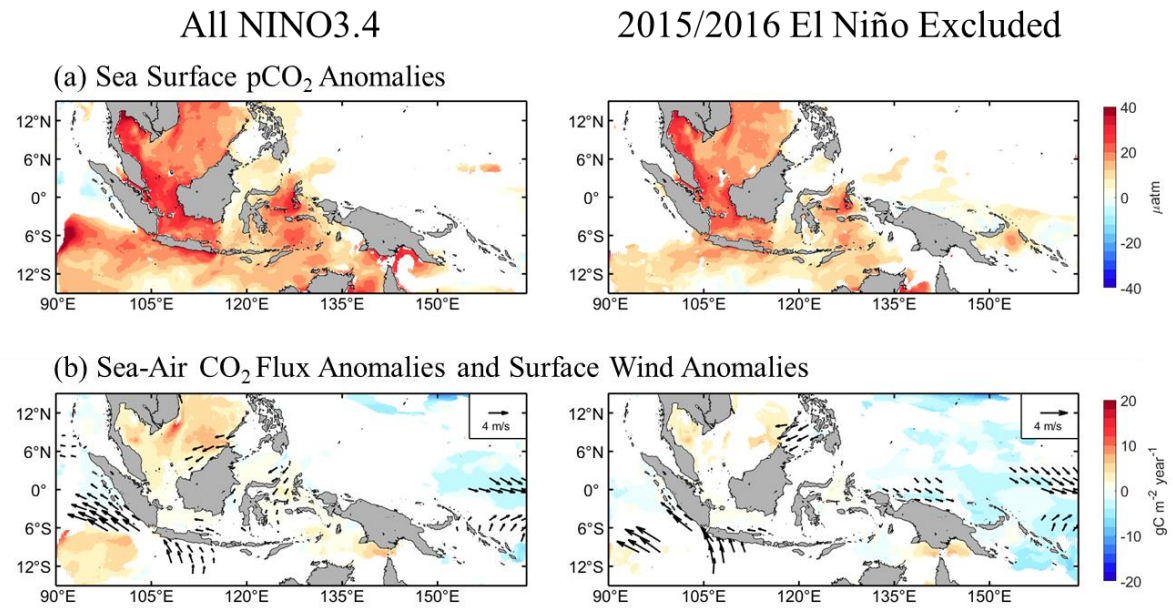

Figure 8. November–March (a) regressed sea surface pCO_2 anomalies (in µatm) and (b) regressed sea–air CO_2 flux anomalies (in gC m^{-2} $year^{-1}$) along with wind anomalies (Vector arrows, in m/s) against one–standard deviation of NINO3.4 (1σNINO3.4) at zero–lag. Regression was calculated after separating IOD effect on ENSO. Shaded colours and vector arrows are significant at $p < 0.01$.

Despite regressed sea surface pCO_2 anomalies against DMI, which showed a magnitude comparable to the NINO3.4–regressed value which about +40 µatm $(1\sigma DMI)^{-1}$, the regressed sea–air CO_2 flux anomalies against DMI showed a much higher value. Regressed sea–air CO_2 flux anomalies against the DMI showed value as high as +20 gC m^{-2} $year^{-1}(1\sigma DMI)^{-1}$. Removing the 2019 pIOD events from the regression analysis (Figure 9, second column) resulted in only slight changes in both sea surface pCO_2 anomalies and sea–air CO_2 flux anomalies associated with IOD. This implies that even a typical IOD event (after the ENSO influence has been removed) could trigger strong anomalies in the sea–air CO_2 flux, especially around the south of Java.

https://doi.org/10.5194/egusphere-2022-1067
Preprint. Discussion started: 14 October 2022
© Author(s) 2022. CC BY 4.0 License.

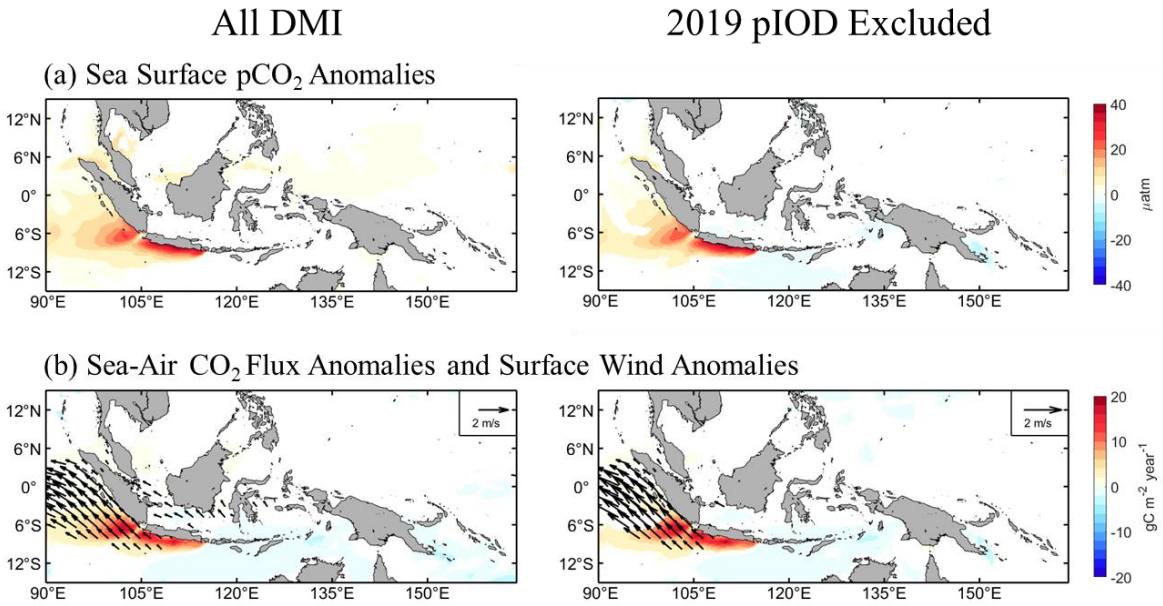

Figure 9. July–November (a) regressed sea surface pCO_2 anomalies (in μatm) and (b) regressed CO_2 flux anomalies (in gC m^{-2}. $year^{-1}$) along with wind anomalies (Vector, in m/s) against one–standard deviation of DMI (1σDMI) at zero–lag. Regression was calculated after separating ENSO effect on IOD. Shaded colours and vector arrows are significant at $p < 0.01$.

4 Discussion

Examination of long–term sea–air CO_2 exchange in the TMC requires careful consideration. Global sea surface pCO_2 and sea–air CO_2 flux reconstruction based on neural network approach (Landschützer et al., 2016) or empirical model (Iida et al., 2021) shows opposite atmospheric CO_2 sink/source characteristic with observations–based study (Hamzah et al., 2020; Kartadikaria et al., 2015). Lack of continuous observation system (e.g., open ocean mooring) in the area create additional constraint to decide the true atmospheric CO_2 sink/source characteristic of the region. Our coupled OGCM simulation experiment on the other hand, showed consistent results with those observations–based study within the TMC and other model with higher complexity. Consistency in the CO_2 sink/source characteristic shown by our simulation experiment enabled us to further analyse the produced sea–air CO_2 exchange variabilities in response to the climatic forcing over the 2010–2019 period. Biases in open ocean as shown previously can be associated to the excess alkalinity in the surface that still underestimated in the model. This was supported by the fact that the model domain is still within the Indo–Pacific warm pool region with small horizontal SST gradient which should results in similar thermally forced sea surface pCO_2. Further model improvement to address this issue by enhancing the excess alkalinity gradient between TMC and its adjacent open ocean is subject to upcoming studies.

While acted as full–year net atmospheric CO_2 source, particularly inside the TMC, our simulation results indicated pronounced seasonality around the South of Java. Strong seasonal winds that triggered upwelling around the area during

https://doi.org/10.5194/egusphere-2022-1067
Preprint. Discussion started: 14 October 2022
© Author(s) 2022. CC BY 4.0 License.

autumn (Horii et al., 2018; Ningsih et al., 2013: Siswanto et al., 2020; Susanto et al., 2001) created favourable conditions for strong CO_2 degassing through a combination of accelerated gas exchange and an abundant supply of subsurface inorganic carbon. This mechanism was not apparent in other areas across the TMC, making it a unique feature from the sea–air CO_2 exchange perspective. Note that the aggregate results of upwelling to the sea–air CO_2 exchange might vary across regions (Chakraborty et al., 2018; Valsala et al., 2014) and thus, the results presented by this model for the South of Java should not be taken as a generalization for all upwelling–active regions.

An attempt to elucidate the extent of extreme climate events (2015/2016 El Niño and 2019 pIOD) influence on the sea–air CO_2 exchange across the TMC through regression analysis yielded notable results. In agreement with the suggestion by Kartadikaria et al. (2015), regression analysis suggested a lower–than–usual sea surface pCO_2 during La Niña and *vice versa* during El Niño. The sea–air CO_2 flux modulation under ENSO influence interestingly, did not necessarily follow the sea surface pCO_2 modulation spatial pattern and relatively weaker than under IOD influence. This can be attributed to different modulation tendency caused by the two climatic forcings.

Weaker (stronger) northwest monsoon circulation within the TMC during El Niño (La Niña) due to anomalous divergence (convergence) in the western Pacific could weaken (strengthen) the gas exchange between the sea surface and the atmosphere. However, shifts in the Walker circulation (Alexander et al., 2002) caused by the same anomalous divergence (convergence) also altered the cloud distribution across the tropics, including the TMC itself, and affected SST. Decreased (increased) cloud cover around the TMC during El Niño (La Niña) can increase (decrease) SST through an increase (decrease) in incoming solar radiation. This mechanism could increase (decrease) sea surface pCO_2 and ultimately strengthen (weaken) CO_2 degassing. The opposite modulation tendencies between atmospheric and oceanic conditions in response to ENSO forcing made the CO_2 flux anomalies magnitude associated with ENSO less pronounced, despite the strong sea surface pCO_2 anomalies.

Conversely, the IOD did not exhibit such opposite tendencies, which resulted in the strong linearity between the sea surface pCO_2 anomalies and the sea–air CO_2 flux anomalies. Typical IOD events occur between late summer–autumn, where seasonal upwelling occurs (Delman et al., 2016; 2018; Susanto et al., 2001). Anomalous south–easterly (north–westerly) winds during the pIOD (nIOD) around SETIO can directly modulate upwelling around the south of Java. Enhanced (suppressed) upwelling in response to stronger (weaker) wind forcing during pIOD (nIOD) then result in higher (lower)–than–usual sea surface pCO_2 from the ocean side and accelerated (decelerated) gas exchange on the atmospheric side.

Exclusion of extreme climate events (i.e., 2015/16 El Nino and 2019 pIOD) in the regression analysis implies the events were likely responsible for a larger extent of sea–air CO_2 exchange modulation around the TMC over the last decade. Significant difference in regressed sea–air CO_2 flux anomalies after exclusion of 2015/16 El Niño despite the existence of strong 2010–2012 La Niña emphasizes the peculiarities of the recent extreme El Niño event. The 2010–2012 La Niña shows comparable magnitude with the 2015/16 El Niño as indicated by the Multivariate ENSO Index v2 (MEIv2; Zhang et al., 2019). It is possible that the Pacific decadal climatic shift in the 2010s modified the ENSO flavour, as pointed out by Newman et al. (2016), including its influence on the TMC, so that sea–air CO_2 flux modulation related to the 2015/2016 El

https://doi.org/10.5194/egusphere-2022-1067
Preprint. Discussion started: 14 October 2022
© Author(s) 2022. CC BY 4.0 License.

Niño showed substantially different characteristics. Further modelling studies across the TMC over a longer time–scale will be needed to confirm this possible decadal variation in the sea–air CO_2 exchange. Considering the simulation results and analysis conducted here, pronounced modulation of the sea–air CO_2 exchange across the TMC in the future can be expected, as recent studies have indicated an intensification of extreme climate anomalies under the effect of greenhouse gas forcing (Cai et al., 2018; Grothe et al., 2019; Zhang et al., 2018).

Finally, one of the biggest challenges hindering this study was that we have not incorporate river discharge in the simulation experiment. The lack of reliable datasets, especially for carbonate chemistry–related parameters, such as total DIC, total alkalinity, and nutrients, as highlighted by Valsala et al. (2014), was the main reason for this limitation. Such data are critical for evaluating the robustness of any regional–scale watershed modelling effort before further use in coupled OGCM–ecosystem models. Incorporating river discharge inappropriately for studying upper–ocean carbon cycle variability will only produce questionable results. DIC concentration from river discharge, for example, varies widely between river mouths, with values ranging from 284 µmol kg^{-1} (Rosentreter and Eyre, 2019) to as high as 3,500 µmol kg^{-1} (Kawahata et al., 2000). This highly variable value did not include the possible strong seasonal and interannual variability of the river–discharged material, as presumed by Xiu and Chai (2014).

5 Conclusion

This study presents results from high–resolution coupled OGCM with low–trophic ecosystem simulation experiment focusing on sea–air CO_2 exchange variabilities across the TMC, a region regarded as undersampled (Hamzah et al., 2020) and usually overlooked by global–scale modelling and/or reconstruction efforts. Compared with available reconstruction product, simulated atmospheric CO_2 sink/source characteristic within the TMC from this modelling study agreed with previous observation–based studies (Hamzah et al., 2020; Kartadikaria et al., 2015) where the region acts as net atmospheric CO_2 source. Further, we also analysed the interannual variations of sea–air CO_2 exchange under Indo–Pacific climatic forcing over the 2010–2019 period along with its possible mechanism from sea–air interaction perspective. This has never been done before considering the aforementioned limitations. Generally, the CO_2 degassing anomalies showed in–phase relationship with both IOD and ENSO (i.e., positive sea–air CO_2 flux anomalies during positive phase of IOD or ENSO, and *vice versa*). The ENSO tends to induce larger scale of sea–air CO_2 flux modulation while the IOD showed confined influence around South of Java but with higher magnitude of modulation. It was further suggested that the latest extreme climate event such as the 2015/2016 El Niño and 2019 pIOD were responsible for slowing the secular trend in the CO_2 degassing to atmosphere from the region. While results presented may provide insight about sea-air CO_2 exchange variabilities in TMC, it can be utilized also to invite interdisciplinary research collaborations regarding establishment of a continuous sea–air CO_2 exchange monitoring system across the region and enrich our understanding of its dynamics under changing environments.

https://doi.org/10.5194/egusphere-2022-1067
Preprint. Discussion started: 14 October 2022
© Author(s) 2022. CC BY 4.0 License.

Code Availability

The original code of our model and necessary code to prepare the input for simulation experiment can be accessed at https://github.com/NakamuraTakashi.

Data Availability

Authors declare that all the data used in this study area publicly available. The Surface Ocean CO_2 Atlas (SOCAT) datasets can be accessed through https://www.socat.info. Global sea surface temperature from HadISST1.1 used for calculating the NINO3.4 and DMI can be retrieved from https://www.metoffice.gov.uk/hadobs/hadisst/. Global sea surface pCO_2 and sea–air CO_2 flux reconstruction from Japan Meteorological Agency (JMA) and can be retrieved from https://www.data.jma.go.jp/gmd/kaiyou/english/co2_flux/co2_flux_data_en.html. Global sea surface pCO_2 and sea–air CO_2 flux using two–step neural network produced by the Max Planck Institute can be obtained from https://www.nodc.noaa.gov/archive/arc0105/0160558/3.3/data/0–data/

Author Contributions

FA and TN designed the study and conduct the numerical experiment. AW and ARK provided pCO_2 observation data within the study area and help interpret the results. KN acquired the funding. FA wrote the original draft of the manuscript. All authors have read and give their review and comment to improve the final manuscript.

Competing Interest

The authors declare that they have no conflict of interest

Disclaimer

Publisher's note: Copernicus Publications remains neutral with regard to jurisdictional claims in published maps and institutional affiliations.

Acknowledgement

This study was funded by Science and Technology Research Partnership for Sustainable Development through the "Comprehensive Assessment and Conservation of Blue Carbon Ecosystem and their Services in the Coral Triangle (BlueCARES)" Project. The first author is a scholarship recipient from Japan's ministry of education, culture, sports, science,

© Author(s) 2022. CC BY 4.0 License.

and technology (MEXT). We are grateful for the high–performance computing services 'TSUBAME 3.0' provided by the Tokyo Institute of Technology for making this simulation experiment possible.

References

Alexander, M. A., Bladé, I., Newman, M., Lanzante, J. R., Lau, N. C., and Scott, J. D.: The atmospheric bridge: The influence of ENSO teleconnections on air–sea interaction over the global oceans. Journal of Climate, 15(16), 2205–2231. https://doi.org/10.1175/1520–0442(2002)015<2205:TABTIO>2.0.CO;2 , 2002

Arteaga, L., Pahlow, M., & Oschlies, A.: Modeled Chl:C ratio and derived estimates of phytoplankton carbon biomass and its contribution to total particulate organic carbon in the global surface ocean. Global Biogeochemical Cycles, 30(12), 1791–1810. https://doi.org/10.1002/2016GB005458, 2016

Ashok, K., Guan, Z., & Yamagata, T.: A look at the relationship between the ENSO and the Indian Ocean Dipole. Journal of the Meteorological Society of Japan. https://doi.org/10.2151/jmsj.81.41, 2003

Ashok, K., Behera, S. K., Rao, S. A., Weng, H., & Yamagata, T.: El Niño Modoki and its possible teleconnection. Journal of Geophysical Research: Oceans. https://doi.org/10.1029/2006JC003798 , 2007

Bakker, D. C. E., Pfeil, B., Landa, C. S., Metzl, N., O'Brien, K. M., Olsen, A., Smith, K., Cosca, C., Harasawa, S., Jones, S. D., Nakaoka, S., Nojiri, Y., Schuster, U., Steinhoff, T., Sweeney, C., Takahashi, T., Tilbrook, B., Wada, C., Wanninkhof, R., Alin, S. R., Balestrini, C. F., Barbero, L., Bates, N. R., Bianchi, A. A., Bonou, F., Boutin, J., Bozec, Y., Burger, E. F., Cai, W.–J., Castle, R. D., Chen, L., Chierici, M., Currie, K., Evans, W., Featherstone, C., Feely, R. A., Fransson, A., Goyet, C., Greenwood, N., Gregor, L., Hankin, S., Hardman–Mountford, N. J., Harlay, J., Hauck, J., Hoppema, M., Humphreys, M. P., Hunt, C. W., Huss, B., Ibánhez, J. S. P., Johannessen, T., Keeling, R., Kitidis, V., Körtzinger, A., Kozyr, A., Krasakopoulou, E., Kuwata, A., Landschützer, P., Lauvset, S. K., Lefèvre, N., Lo Monaco, C., Manke, A., Mathis, J. T., Merlivat, L., Millero, F. J., Monteiro, P. M. S., Munro, D. R., Murata, A., Newberger, T., Omar, A. M., Ono, T., Paterson, K., Pearce, D., Pierrot, D., Robbins, L. L., Saito, S., Salisbury, J., Schlitzer, R., Schneider, B., Schweitzer, R., Sieger, R., Skjelvan, I., Sullivan, K. F., Sutherland, S. C., Sutton, A. J., Tadokoro, K., Telszewski, M., Tuma, M., van Heuven, S. M. A. C., Vandemark, D., Ward, B., Watson, A. J., and Xu, S.: A multi–decade record of high–quality fCO_2 data in version 3 of the Surface Ocean CO_2 Atlas (SOCAT), Earth Syst. Sci. Data, 8, 383–413, https://doi.org/10.5194/essd–8–383–2016, 2016.

Cai, W., Wang, G., Gan, B., Wu, L., Santoso, A., Lin, X., et al. (2018). Stabilised frequency of extreme positive Indian Ocean Dipole under 1.5°C warming. Nature Communications, 9(1), 4–11. https://doi.org/10.1038/s41467–018–03789–6 , 2018

Cai, W., Wu, L., Lengaigne, M., Li, T., McGregor, S., Kug, J. S., et al.: Pantropical climate interactions. Science, 363(6430). https://doi.org/10.1126/science.aav4236 , 2019

https://doi.org/10.5194/egusphere-2022-1067
Preprint. Discussion started: 14 October 2022
© Author(s) 2022. CC BY 4.0 License.

Chai, F., Liu, G., Xue, H., Shi, L., Chao, Y., Tseng, C. M., et al.: Seasonal and interannual variability of carbon cycle in South China Sea: A three–dimensional physical–biogeochemical modeling study. Journal of Oceanography. https://doi.org/10.1007/s10872–009–0061–5 , 2009

Chakraborty, K., Valsala, V., Gupta, G. V. M., & Sarma, V. V. S. S.: Dominant Biological Control Over Upwelling on pCO_2 in Sea East of Sri Lanka. Journal of Geophysical Research: Biogeosciences, 123(10), 3250–3261. https://doi.org/10.1029/2018JG004446, 2018

Chassignet, E. P., Hurlburt, H. E., Smedstad, O. M., Halliwell, G. R., Hogan, P. J., Wallcraft, A. J., and Bleck, R.: Ocean prediction with the Hybrid Coordinate Ocean Model (HYCOM). In Ocean Weather Forecasting: An Integrated View of Oceanography. https://doi.org/10.1007/1–4020–4028–8_16 , 2006

Delman, A. S., Sprintall, J., McClean, J. L., and Talley, L. D.: Anomalous Java cooling at the initiation of positive Indian Ocean Dipole events. Journal of Geophysical Research: Oceans. https://doi.org/10.1002/2016JC011635 , 2016

Delman, A. S., McClean, J. L., Sprintall, J., Talley, L. D., and Bryan, F. O.: Process–Specific Contributions to Anomalous Java Mixed Layer Cooling During Positive IOD Events. Journal of Geophysical Research: Oceans, 123(6), 4153–4176. https://doi.org/10.1029/2017JC013749, 2018

Egbert, G. D. and Erofeeva, S. Y.: Efficient inverse modeling of barotropic ocean tides, J. Atmos. Ocean. Technol., 19, 183–204, https://doi.org/10.1175/1520-0426(2002)019<0183:EIMOBO>2.0.CO;2, 2002.

Gordon, A. L.: Interocean exchange of thermocline water. Journal of Geophysical Research. https://doi.org/10.1029/jc091ic04p05037, 1986

Gregg, W. W., and Casey, N. W.: Modeling coccolithophores in the global oceans. Deep–Sea Research Part II: Topical Studies in Oceanography. https://doi.org/10.1016/j.dsr2.2006.12.007, 2007

Grothe, P. R., Cobb, K. M., Liguori, G., Di Lorenzo, E., Capotondi, A., Lu, Y., et al.: Enhanced El Niño–Southern Oscillation Variability in Recent Decades. Geophysical Research Letters, 47(7), 1–8. https://doi.org/10.1029/2019GL083906 , 2020

Hamzah, F., Agustiadi, T., Susanto, R. D., Wei, Z., Guo, L., Cao, Z., and Dai, M.: Dynamics of the Carbonate System in the Western Indonesian Seas During the Southeast Monsoon. Journal of Geophysical Research: Oceans. https://doi.org/10.1029/2018JC014912 , 2020

Horii, T., Ueki, I., and Ando, K.: Coastal upwelling events along the southern coast of Java during the 2008 positive Indian Ocean Dipole. Journal of Oceanography, 74(5), 499–508. https://doi.org/10.1007/s10872–018–0475–z, 2018

Hu, C., Lee, Z., and Franz, B.: Chlorophyll a algorithms for oligotrophic oceans: A novel approach based on three–band reflectance difference. Journal of Geophysical Research: Oceans. https://doi.org/10.1029/2011JC007395 , 2012

Iida Y., Takatani, Y., Kojima, A., and Ishii, M.: Global trends of ocean CO_2 sink and ocean acidification: An obsevation–based reconstruction of surface ocean inorganic carbon variables. Journal of Oceanography. 77, 323–358, https://doi.org/10.1007/s10872-020-00571-5, 2021

https://doi.org/10.5194/egusphere-2022-1067
Preprint. Discussion started: 14 October 2022
© Author(s) 2022. CC BY 4.0 License.

Ishizu, M., Miyazawa, Y., Tsunoda, T., and Guo, X.: Development of a biogeochemical and carbon model related to ocean acidification indices with an operational ocean model product in the North Western Pacific. Sustainability (Switzerland), 11(9). https://doi.org/10.3390/su11092677, 2019

Ishizu, M., Miyazawa, Y., Tsunoda, T., and Guo, X.: Seasonal variability in the inorganic ocean carbon cycle in the Northwest Pacific evaluated using a biogeochemical and carbon model coupled with an operational ocean model. Climatic Change. https://doi.org/10.1007/s10584–020–02779–2 , 2020

Jansen, H., Zeebe, R. E., and Wolf–Gladrow, D. A.: Modeling the dissolution of settling CaCO3 in the ocean. Global Biogeochemical Cycles, 16(2), 11–1–11–16. https://doi.org/10.1029/2000gb001279 , 2022

Kartadikaria, A. R., Watanabe, A., Nadaoka, K., Adi, N. S., Prayitno, H. B., Soemorumekso, S., Muchtar, M., Triyulianti, I., Setiawan, A., Suratno, S., & Khasanah, E. N.: CO_2 sink/source characteristics in the tropical Indonesian seas. Journal of Geophysical Research: Oceans. https://doi.org/10.1002/2015JC010925 , 2015

Kawahata, H., Yukino, I., and Suzuki, A.: Terrestrial influences on the Shiraho fringing reef, Ishigaki Island, Japan: High carbon input relative to phosphate. Coral Reefs, 19(2), 172–178. https://doi.org/10.1007/s003380000093 , 2000

Key, R. M., Kozyr, A., Sabine, C. L., Lee, K., Wanninkhof, R., Bullister, J. L., et al.: A global ocean carbon climatology: Results from Global Data Analysis Project (GLODAP). Global Biogeochemical Cycles, 18(4), 1–23. https://doi.org/10.1029/2004GB002247 , 2004

Kobayashi, S., Ota, Y., Harada, Y., Ebita, A., Moriya, M., Onoda, H., et al.: The JRA–55 reanalysis: General specifications and basic characteristics. Journal of the Meteorological Society of Japan, 93(1), 5–48. https://doi.org/10.2151/jmsj.2015–001 , 2015

Krumhardt, K. M., Lovenduski, N. S., Iglesias–Rodriguez, M. D., and Kleypas, J. A.: Coccolithophore growth and calcification in a changing ocean. Progress in Oceanography, 159(June), 276–295. https://doi.org/10.1016/j.pocean.2017.10.007 , 2017

Krumhardt, K. M., Lovenduski, N. S., Long, M. C., Levy, M., Lindsay, K., Moore, J. K., and Nissen, C.: Coccolithophore Growth and Calcification in an Acidified Ocean: Insights from Community Earth System Model Simulations. Journal of Advances in Modeling Earth Systems, 11(5), 1418–1437. https://doi.org/10.1029/2018MS001483, 2019

Landschützer, P., Gruber, N., and Bakker, D. C. E.: Decadal variations and trends of the global ocean carbon sink. Global Biogeochemical Cycles, 30(10), 1396–1417. https://doi.org/10.1002/2015GB005359, 2016

Li, Y., Chen, Q., Liu, X., Li, J., Xing, N., Xie, F., et al.: Long–Term Trend of the Tropical Pacific Trade Winds Under Global Warming and Its Causes. Journal of Geophysical Research: Oceans, 124(4), 2626–2640. https://doi.org/10.1029/2018JC014603 , 2019

Lu, B., and Ren, H. L.: What Caused the Extreme Indian Ocean Dipole Event in 2019? Geophysical Research Letters. https://doi.org/10.1029/2020GL087768 , 2020

© Author(s) 2022. CC BY 4.0 License.

Martiny, A. C., Vrugt, J. A., & Lomas, M. W.: Concentrations and ratios of particulate organic carbon, nitrogen, and phosphorus in the global ocean. Scientific Data, 1, 1–7. https://doi.org/10.1038/sdata.2014.48 , 2014

Mathis, M., Logemann, K., Maerz, J., Lacroix, F., Hagemann, S., Chegini, F., Ramme, L., Ilyina, T., Korn, P., and Schrum, C.: Seamless Integration of the Coastal Ocean in Global Marine Carbon Cycle Modeling. Journal of Advances in Modeling Earth Systems, 14(8). https://doi.org/10.1029/2021MS002789 , 2022

Najjar, R. G., and J. C. Orr (1999), Biotic–HOWTO, internal OCMIP report, 15 pp., LSCE/CEA Saclay, Gif–sur–Yvette, France.

Nakamura, T., Nadaoka, K., Watanabe, A., Yamamoto, T., Miyajima, T., and Blanco, A. C.: Reef–scale modeling of coral calcification responses to ocean acidification and sea–level rise. Coral Reefs, 37(1), 37–53. https://doi.org/10.1007/s00338–017–1632–3 , 2018

Newman, M., Alexander, M. A., Ault, T. R., Cobb, K. M., Deser, C., Di Lorenzo, E., et al.: The Pacific decadal oscillation, revisited. Journal of Climate, 29(12), 4399–4427. https://doi.org/10.1175/JCLI–D–15–0508.1 , 2016

Ningsih, N. S., Rakhmaputeri, N., and Harto, A. B.: Upwelling variability along the southern coast of Bali and in Nusa Tenggara waters. Ocean Science Journal, 48(1), 49–57. https://doi.org/10.1007/s12601–013–0004–3 , 2013

Obata, A., and Kitamura, Y.: Interannual variability of the sea–air exchange of CO_2 from 1961 to 1998 simulated with a global ocean circulation–biogeochemistry model. Journal of Geophysical Research: Oceans. https://doi.org/10.1029/2001jc001088 , 2003

Pujiana, K., McPhaden, M. J., Gordon, A. L., and Napitu, A. M.: Unprecedented Response of Indonesian Throughflow to Anomalous Indo–Pacific Climatic Forcing in 2016. Journal of Geophysical Research: Oceans, 124(6), 3737–3754. https://doi.org/10.1029/2018JC014574 , 2019

Pujiana, K., and McPhaden, M. J.: Intraseasonal Kelvin Waves in the Equatorial Indian Ocean and Their Propagation into the Indonesian Seas. Journal of Geophysical Research: Oceans. https://doi.org/10.1029/2019JC015839 , 2020

Rayner, N. A., Parker, D. E., Horton, E. B., Folland, C. K., Alexander, L. V., Rowell, D. P., et al.: Global analyses of sea surface temperature, sea ice, and night marine air temperature since the late nineteenth century. Journal of Geophysical Research: Atmospheres, 108(14). https://doi.org/10.1029/2002jd002670 , 2003

Redfield, A.C.: On the Proportion of Organic Derivatives in Sea Water and Their Relation to The Composition of Plankton. James Johnstone Memorial Volume, 176–192 , 1934

Rosentreter, J. A., and Eyre, B. D.: Alkalinity and dissolved inorganic carbon exports from tropical and subtropical river catchments discharging to the Great Barrier Reef, Australia. Hydrological Processes, 34(7), 1530–1544. https://doi.org/10.1002/hyp.13679 , 2020

Saji, N. H., Goswami, P. N., Vinayachandran, P. N., and Yamagata, T.:A dipole mode in the tropical indain ocean. Nature, 401(September), 360–363. https://doi.org/10.1038/43854 , 1999

https://doi.org/10.5194/egusphere-2022-1067
Preprint. Discussion started: 14 October 2022
© Author(s) 2022. CC BY 4.0 License.

Saji, N. H., & Yamagata, T.: Possible impacts of Indian Ocean Dipole mode events on global climate. Climate Research. https://doi.org/10.3354/cr025151 , 2003

Sarmiento, J.L., Gruber, N.: Ocean Biogeochemical Dynamics. Princeton U. Press. ISBN 978–0–691–01707–5, 2006

Shchepetkin, A. F., and McWilliams, J. C.: The regional oceanic modeling system (ROMS): A split–explicit, free–surface, topography–following–coordinate oceanic model. Ocean Modelling, 9(4), 347–404. https://doi.org/10.1016/j.ocemod.2004.08.002, 2005

Siswanto, E., Horii, T., Iskandar, I., Gaol, J. L., Setiawan, R. Y., and Susanto, R. D.: Impacts of climate changes on the phytoplankton biomass of the Indonesian Maritime Continent. Journal of Marine Systems. https://doi.org/10.1016/j.jmarsys.2020.103451, 2020

Susanto, R. D., Gordon, A. L., and Zheng, Q.: Upwelling along the coasts of Java and Sumatra and its relation to ENSO. Geophysical Research Letters. https://doi.org/10.1029/2000GL011844 , 2001

Sutton, A. J., Wanninkhof, R., Sabine, C. L., Feely, R. A., Cronin, M. F., and Weller, R. A.: Variability and trends in surface seawater pCO_2 and CO_2 flux in the Pacific Ocean. Geophysical Research Letters, 44(11), 5627–5636. https://doi.org/10.1002/2017GL073814 , 2017b

Sprintall, J., Gordon, A. L., Koch–Larrouy, A., Lee, T., Potemra, J. T., Pujiana, K., and Wijffels, S. E.: The Indonesian seas and their role in the coupled ocean–climate system. Nature Geoscience. https://doi.org/10.1038/ngeo2188 , 2014

Syamsudin, F., Kaneko, A., and Haidvogel, D. B.: Numerical and observational estimates of Indian Ocean Kelvin wave intrusion into Lombok Strait. Geophysical Research Letters. https://doi.org/10.1029/2004GL021227 , 2004

Takahashi, T., Olafsson, J., Goddard, J. G., Chipman, D. W., and Sutherland, S. C.: Seasonal Variation of CO_2 and Nutrients in the High–Latitude Surface Oceans: A Comparative Study. Global Biogeochemical Cycles. (Vol. 7, Issue 4). https://doi.org/10.1029/93GB02263 , 1993

Takahashi, T., Sutherland, S. C., Sweeney, C., Poisson, A., Metzl, N., Tilbrook, B., et al.: Global sea–air CO_2 flux based on climatological surface ocean pCO_2, and seasonal biological and temperature effects. Deep–Sea Research Part II: Topical Studies in Oceanography. https://doi.org/10.1016/S0967–0645(02)00003–6 , 2002

Takahashi, T., Sutherland, S. C., Wanninkhof, R., Sweeney, C., Feely, R. A., Chipman, D. W., et al.: Climatological mean and decadal change in surface ocean pCO_2, and net sea–air CO_2 flux over the global oceans. Deep–Sea Research Part II: Topical Studies in Oceanography. https://doi.org/10.1016/j.dsr2.2008.12.009 , 2009

Valsala, V. K., Roxy, M. K., Ashok, K., and Murtugudde, R.: Spatiotemporal characteristics of seasonal to multidecadal variability of pCO_2 and air–sea CO_2 fluxes in the equatorial Pacific Ocean. Journal of Geophysical Research: Oceans. https://doi.org/10.1002/2014JC010212 , 2014

Wanninkhof, R.: Relationship between wind speed and gas exchange over the ocean. Journal of Geophysical Research, 97(C5), 7373–7382. https://doi.org/10.1029/92JC00188 , 1992

https://doi.org/10.5194/egusphere-2022-1067
Preprint. Discussion started: 14 October 2022
© Author(s) 2022. CC BY 4.0 License.

Weiss, R.F.: Carbon Dioxide in Water and Seawater: The Solubility of a Non–Ideal Gas. Marine Chemistry, 2(1974), 203–2015. https://doi.org/10.1016/0304–4203(74)90015–2 , 1074

Warner, J. C., Armstrong, B., He, R., and Zambon, J. B.: Development of a Coupled Ocean–Atmosphere–Wave–Sediment Transport (COAWST) Modeling System. Ocean Modelling, 35(3), 230–244. https://doi.org/10.1016/j.ocemod.2010.07.010 , 2010

Weiss, R.F.: Carbon Dioxide in Water and Seawtaer: The Solubility of A Non–Ideal Gas. Marine Chemistry, 2(1974), 203–2015. https://doi.org/10.1016/0304–4203(74)90015–2, 1974

Wyrtki, K.: Physical Oceanography of the Southeast Asian Waters. Naga Report Volume 2. Scientific Results of Marine Investigation of the South China Sea and the Gulf of Thailand 1959–1961. 1961

Xiu, P., and Chai, F.: Variability of oceanic carbon cycle in the North Pacific from seasonal to decadal scales. Journal of Geophysical Research: Oceans, 119(8), 5270–5288. https://doi.org/10.1002/2013jc009505 , 2014

Zhang, L., Du, Y., and Cai, W.: Low–Frequency Variability and the Unusual Indian Ocean Dipole Events in 2015 and 2016. Geophysical Research Letters, 45(2), 1040–1048. https://doi.org/10.1002/2017GL076003 , 2018

Zhang, T., Hoell, A., Perlwitz, J., Eischeid, J., Murray, D., Hoerling, M., and Hamill, T. M.: Towards Probabilistic Multivariate ENSO Monitoring. Geophysical Research Letters, 46(17–18), 10532–10540. https://doi.org/10.1029/2019GL083946s , 2019